Article

Thermochemical Analysis of a Packed-Bed Reactor Using Finite Elements with FlexPDE and COMSOL Multiphysics

Sebastian Taco-Vasquez [1]*, César A. Ron [1], Herman A. Murillo [1], Andrés Chico [1] and Paul G. Arauz [2]

[1] Department of Chemical Engineering, Escuela Politécnica Nacional, Quito 170517, Ecuador; cesar.ron@epn.edu.ec (C.A.R.); herman.murillo@epn.edu.ec (H.A.M.); andres.chico@epn.edu.ec (A.C.)

[2] Department of Mechanical Engineering, Universidad San Francisco de Quito, Quito 170901, Ecuador; parauz@usfq.edu.ec

* Correspondence: sebastian.taco@epn.edu.ec

Abstract: This work presents the thermochemical analysis of a packed-bed reactor via multi-dimensional CFD modeling using FlexPDE and COMSOL Multiphysics. The temperature, concentration, and reaction rate profiles for methane production following the Fischer–Tropsch (F-T) synthesis were studied. To this end, stationary and dynamic differential equations for mass and heat transfer were solved via the finite element technique. The transport equations for 1-D and 2-D models using FlexPDE consider dispersion models, where the fluid and the catalyst can be treated as either homogeneous or heterogenous systems depending on the gradient extents. On the other hand, the 3-D model obtained in COMSOL deems the transport equations incorporated in the Porous Media module. The aim was to compare the FlexPDE and COMSOL models, and to validate them with experimental data from literature. As a result, all models were in good agreement with experimental data, especially for the 2-D and 3-D dynamic models. In terms of kinetics, the predicted reaction rate profiles from the COMSOL model and the 2-D dynamic model followed the temperature trend, thus reflecting the temperature dependence of the reaction. Based on these findings, it was demonstrated that applying different approaches for the CFD modeling of F-T processes conducts reliable results.

Keywords: multi-dimensional CFD modeling; Fischer-Tropsch synthesis; reactor modeling; solid catalysts; heat transfer; kinetics

1. Introduction

Most processes employ beds for the solid phase in the reactor design for fluids flowing through solid catalysts. There are fluidized beds that allow for working at temperatures distributed uniformly alongside the bed and allow the catalyst to regenerate. However, their operation's high costs and complexity make fluidized beds suitable only for being employed regarding a few industrial processes. The other option is to use fixed beds (also called packed beds), whose advantage, other than being cheaper, is that separation of phases after the operation is more effortless [1]. These reactors must control main parameters, such as pressure drop and heat transfer between reactants and catalysts. Single-packed beds are usually employed for adiabatic processes. Still, when there are highly exothermic reactions, shell and tubes packed beds (multi-tubular) are preferred due to their high heat transfer. In the packed-bed reactor diameter, bigger diameters will worsen the heat transfer, and hot spots will occur. In contrast, a small diameter allows for a better heat transfer and reduces the temperature gradient between the center and the reactor wall. Although fluidized beds can have five to ten times greater heat transfer than a packed-bed reactor, allowing isothermal conditions [2], other drawbacks are related to catalyst losses because of catalyst transportation between the reactor and regenerator.

Consequently, it is impossible to have a single large diameter tube packed with a catalyst. Instead, the reactor should be made up of several tubes. At the industrial scale, multitube packed-bed reactors have been shown to have some advantages, including a

behavior close to plug flow conditions, improved catalyst retention, catalyst separation not being required, and the feasibility of the process to be scaled up [3]. Still, heat removal is the primary consideration in the design of packed-bed reactors for highly exothermic reactions. It is desired to operate these beds within a range of temperatures to optimize productivity and selectivity [4].

In this context, the tube diameter for exothermic reactions is generally between two and 5 cm [5], and the tube-to-particle diameter is about eight depending on the application [1]. Smaller particles tend to decrease the bed's radial thermal conductivity, causing an excessive pressure drop; however, larger particles cause high intraparticle mass transfer resistances, reducing the heat removal from the catalyst to the fluid. This increases the risk of thermal instability of the particle, also showing hot spots inside the catalyst that can damage it [6]. The pressure drop in a porous medium is crucial within a reacting channel, and it affects the heat transfer coefficient, as it must be modified. Darcy's law is one option to study the existing pressure drop in a porous medium. Accordingly, there are different approaches to link Darcy's law to heat transfer equations (e.g., by the Nusselt number). Shah et al. [7] performed a simulation for an alumina-based nanofluid flowing through a porous cavity. Herein, a model was used that associates the Nusselt number with the Darcy's parameter, which depends on the medium permeability and the channel length.

Efficient heat removal is associated with the catalytic material. For instance, a V-Mo-based catalyst conducting the maleic anhydride production from benzene oxidation at 350 °C was conducted in a multi-tubular reactor with two cm-tubes. Unfortunately, heat removal was not as efficient as expected even when using small tubes, as temperature increments of 100 °C were observed in the shell, which can be transmitted to the tubes [1]. In this context, some authors have investigated catalyst geometries and other strategies to achieve better performance on heat transfer. Visconti et al. [8] and Asalieva et al. [9] prepared cobalt-based catalysts onto metallic supports for the Fischer–Tropsch (F-T) reaction using different geometries and wash-coating methodologies. It resulted in reduced hot spots reaching more isothermal conditions.

The Fischer–Tropsch reaction ($\Delta Hr = -165$ kJ/mol$_{CO}$) is one study case of highly exothermic reactions, which entails the syngas (i.e., a CO/H$_2$ mixture) conversion to long-chain hydrocarbons towards fuel production [10]. The reaction is sensitive to temperature, so a controlled heat transfer inside the reactor is critical to keep selectivity at reasonable levels, as it can be hindered at high temperatures [11].

Modeling and simulation determine design parameters and process operating conditions to optimize their performance and keep the system operating within a safe range. The most critical parameters, apart from kinetics, are those that control radial heat transfer from the packed bed to the cooling tube [12]. Due to the substantial difference between heat transfer parameters measured under reactive and non-reactive conditions reported in the literature, choosing the best correlations that lead to the most accurate evaluation of these parameters is essential.

The existing literature about the modeling of the F-T reaction addresses different approaches. Recently, computational fluid dynamics (CFD) has been performed for modeling this process. Mohammad et al. [13] provided remarkable insights into the CFD modeling of F-T synthesis using microchannel microreactors. These authors investigated the effect of different parameters focusing mainly on the channel design. For example, they found that the maximum temperature observed in the channel can be reduced by increasing the channel width. On the other hand, the configuration of the channels was also studied, resulting in lower productivity losses when setting the channels in a series. However, the authors suggest further analysis of heat removal mechanisms.

Abusrafa et al. [14] developed a 2-D model for comparing a microfibrous F-T reactor to a conventional packed-bed reactor. The thermal performance of both reactors on conversion and hydrocarbon selectivity was assessed. The authors also discussed the scale-up potential of this novel reactor, suggesting that CFD modeling can be considered the first approach to enhance the conventional F-T technologies.

Chabot et al. [15] studied a 2-D pseudo-homogenous model to determine the thermal behavior over cobalt supported on alumina, concluding that liquid hydrocarbon selectivity was decreased when isothermal conditions were not achieved. Na et al. [16] modeled a 2-D axisymmetric microchannel reactor and proposed a genetic algorithm for multi-objective optimization using a cobalt-based catalyst. Their findings indicated that catalyst zone division could increase productivity and decrease temperature increments.

On the other hand, the pressure drops in CFD simulations for porous medium (e.g., considering Darcy's law) is often considered only in the axial direction showing viscous and inertial resistances. Pavlišič et al. [17] used a modified Darcy's law, incorporating the kinetic energy of the fluid to the inertial term in a laminar flow regime for packed-bed reactors. Their simulation results suggest a channeling strategy to decrease induced pressure differences. Nevertheless, Darcy's law is valid for fluid mainly influenced by viscous effects and negligible at higher velocities. In this case, other correlations such as Ergun and Forchheimer can predict the pressure drop as a function of velocity where some terms are added to correct the mentioned drawbacks [18,19].

The modeling of F-T synthesis must also consider the kinetics equations. In this regard, Rai et al. [20] proposed a power law-based kinetic model for microchannel and packed-bed reactors, assuming different reaction orders. The activation energy was lower for the microchannel reactor and reached >92% of CO conversion; however, a lower temperature gradient was found for the packed-bed reactor. In most cases, reaction orders for CO and H_2 were found to be positive, but there was a case following a negative order for CO, which leads to a process inhibition due to the CO absorption by the catalyst.

This paper proposed a multi-dimensional CFD modeling of the F-T reaction in a packed-bed reactor considering temperature and concentration gradients for methane production from syngas as a first approach. Experimental validation was also performed to assess the validity of the proposed models, as indicated in our previous work [21]. According to Deutschmann [22], if the concentration and temperature gradients between the gas and the catalyst are small, a homogeneous model can be used. In contrast, if the gradients are significant, a model for each phase must be applied, considering the mass and heat transport between the fluid phase and the catalyst bed. For instance, when using Ansys Fluent, heat transfer for heterogeneous catalysis is commonly simulated by the non-equilibrium thermal model, as Pessoa et al. [23] address the CFD simulation of packed bed fermentation bioreactor. For the present study, the equations describing the catalyst bed's mass, energy, and reaction transfer were incorporated into the models. 1-D models (along the packed-bed length) can be used when the temperature and concentration gradients on the radial axis are small; otherwise, a 2-D model is used. In this regard, 1-D and 2-D models were developed using FlexPDE. In addition, a 3-D model was attained using COMSOL Multiphysics. Finally, all models were validated with experimental data to assess the accuracy of the proposed models. In the case of the FlexPDE models, dispersion models (i.e., modified transport equations using a dimensional numbers like the Peclet number) were applied to perform the corresponding simulations, whereas the COMSOL model employs the default transport equations defined by the available modules for porous media modeling. As modeling of the F-T synthesis has been previously addressed in the literature, this work intended to further investigate different CFD software to establish the reliability of the available approaches to describe the transport of species in porous media.

2. Model Description

For multitube packed-bed reactors, all tubes should ideally behave the same; this implies that the inlet conditions, wall temperature, concentrations, and temperature profiles are the same. Therefore, we have chosen one cylindrical tube (as indicated in Figure 1) to perform our analysis over a packed-bed reactor. The two spatial variables will be the radial direction (r) and the axial or longitudinal direction (z). The angular direction was not

considered for this simulation since there is no variation in concentration or temperature on the angular axis.
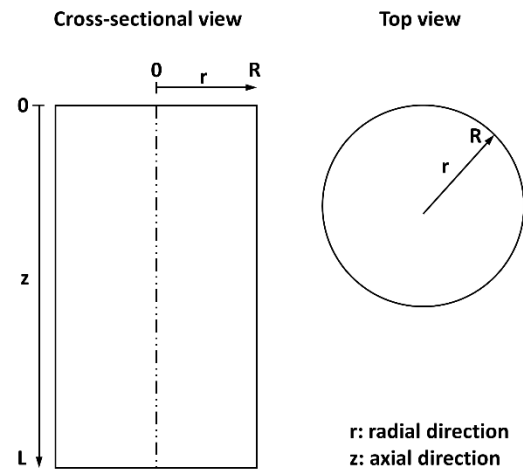

Figure 1. A cross-sectional and top view of a single cylindrical packed-bed reactor.

In this section, the four relevant packed-bed models were discretized: (a) 2-dimensional stationary model; (b) the 1-dimensional dynamic-state model; (c) 2-dimensional dynamic model; and (d) 3-dimensional dynamic model. For models (a), (b), and (c), the governing differential equations were derived and solved using FlexPDE software. On the other hand, model (d) was implemented and solved using COMSOL Multiphysics.

The transport equations, boundary conditions, and the experimental data to validate the proposed models were collected from Skaare [24].

2.1. 2-D stationary Model

It was initially determined that heat and mass transfer are steady-state, as shown in Equations (1) and (2). The temperature $\theta = T/T_o$, and the axes $z' = z/L$ and $r' = r/R$ were discretized.

$$0 = -\frac{\partial \theta}{\partial z'} + \frac{1}{Pe'_{hz}}\frac{\partial^2 \theta}{\partial z'^2} + \frac{1}{Pe'_{hr}}\left[\frac{1}{r'}\frac{\partial}{\partial r'}\left(r'\frac{\partial \theta}{\partial r'}\right)\right] + \frac{L}{u\rho_g C_{pg} T_0}\rho_b \frac{(1-\varepsilon_o)}{(1-\varepsilon_0)}(\Delta H)r_v \qquad (1)$$

$$0 = \frac{\partial y_i}{\partial z'} + \frac{1}{Pe'_{mz}}\frac{\partial^2 y_i}{\partial z'^2} + \frac{1}{Pe'_{mr}}\frac{1}{r'}\frac{\partial}{\partial r'}\left(r'\frac{\partial y_i}{\partial r'}\right) + \frac{L}{u_o C_{0i}}\rho_b \frac{(1-\varepsilon_o)}{(1-\varepsilon_0)}r_{vi} \qquad (2)$$

The boundary conditions are listed from Equations (3)–(8).

$$\frac{\partial \theta}{\partial r} = \frac{\partial y_i}{\partial r} = 0 \text{ When } r = 0, \text{ for all } z \qquad (3)$$

$$-\frac{\partial \theta}{\partial r'} = \frac{UcR}{\lambda_{cr}}(\theta - \theta_c) \text{ When } r = R, \text{ for all } z \qquad (4)$$

$$\frac{\partial y_i}{\partial r'} = 0 \text{ When } r = R, \text{ for all } z \qquad (5)$$

$$\frac{\partial \theta}{\partial z} = Pe'_{hz}(\theta - 1) \text{ When } z = 0, \text{ for all } r \qquad (6)$$

$$\frac{\partial y_i}{\partial z} = Pe'_{mz}(y_i - 1) \text{ When } z = 0, \text{ for all } r \qquad (7)$$

$$\frac{\partial \theta}{\partial z} = \frac{\partial y_i}{\partial z} = 0 \text{ When } z = L, \text{ for all } r \qquad (8)$$

2.2. 1-D Dynamic Model

Likewise, heat and mass equations are shown in Equations (9) and (10), respectively, for dynamic state.

$$\frac{L\varepsilon}{u(3600)} + \frac{L\,cp_s\rho_s\,(1-\varepsilon)}{u\rho_f cp_f\,(3600)}\frac{\partial\theta}{\partial t} =$$
$$-\frac{\partial\theta}{\partial z'} + \frac{1}{Pe'_{hz}}\frac{\partial^2\theta}{\partial z'^2} + \frac{L}{u\rho_g C_{pg}T_0}\rho_b\frac{(1-\varepsilon)}{(1-\varepsilon_0)}(\Delta H)r_v + \frac{4U_c L}{d_t u\rho_g C_{pg}}(\theta - \theta_c)$$

(9)

$$\frac{L\varepsilon}{u(3600)}\frac{\partial y_i}{\partial t} = \frac{\partial y_i}{\partial z'} + \frac{1}{Pe'_{mz}}\frac{\partial^2 y_i}{\partial z'^2} + \frac{L}{uC_{0i}}\rho_b\frac{(1-\varepsilon)}{(1-\varepsilon_0)}r_{vi}$$

(10)

The boundary conditions are listed from Equations (11)–(13).

$$\frac{\partial\theta}{\partial z} = Pe'_{hz}(\theta - 1)\ \text{When}\ z = 0,\ \text{for all}\ r$$

(11)

$$\frac{\partial y_i}{\partial z} = Pe'_{mz}(y_i - 1)\ \text{When}\ z = 0,\ \text{for all}\ r$$

(12)

$$\frac{\partial\theta}{\partial z} = \frac{\partial y_i}{\partial z} = 0\ \text{When}\ z = L,\ \text{for all}\ r$$

(13)

2.3. 2-D Dynamic Model

The heat and mass transfer equations are represented by Equations (14) and (15), respectively, for the 2-dimensional dynamic model.

$$\frac{L\varepsilon}{u(3600)} + \frac{L\,cp_s\rho_s(1-\varepsilon)}{u\rho_f cp_f(3600)}\frac{\partial\theta}{\partial t} =$$
$$-\frac{\partial\theta}{\partial z'} + \frac{1}{Pe'_{hz}}\frac{\partial^2\theta}{\partial z'^2} + \frac{1}{Pe'_{hr}}\left[\frac{1}{r'}\frac{\partial}{\partial r'}\left(r'\frac{\partial\theta}{\partial r'}\right)\right] + \frac{L}{u\rho_g C_{pg}T_0}\rho_b\frac{(1-\varepsilon)}{(1-\varepsilon_0)}(\Delta H)r_v$$

(14)

$$\frac{L\varepsilon}{u(3600)}\frac{\partial y_i}{\partial t} = \frac{\partial y_i}{\partial z'} + \frac{1}{Pe'_{mz}}\frac{\partial^2 y_i}{\partial z'^2} + \frac{1}{Pe'_{mr}}\frac{1}{r'}\frac{\partial}{\partial r'}\left(r'\frac{\partial y_i}{\partial r'}\right) + \frac{L}{uC_{0i}}\rho_b\frac{(1-\varepsilon)}{(1-\varepsilon_0)}r_{vi}$$

(15)

The boundary conditions are listed from Equations (16)–(21).

$$\frac{\partial\theta}{\partial r} = \frac{\partial y_i}{\partial r} = 0\ \text{When}\ r = 0,\ \text{for all}\ z$$

(16)

$$-\frac{\partial\theta}{\partial r'} = \frac{U_c R}{\lambda_{cr}}(\theta - \theta_c)\ \text{When}\ r = R,\ \text{for all}\ z$$

(17)

$$\frac{\partial y_i}{\partial r'} = 0\ \text{When}\ r = R,\ \text{for all}\ z$$

(18)

$$\frac{\partial\theta}{\partial z} = Pe'_{hz}(\theta - 1)\ \text{When}\ z = 0,\ \text{for all}\ r$$

(19)

$$\frac{\partial y_i}{\partial z} = Pe'_{mz}(y_i - 1)\ \text{When}\ z = 0,\ \text{for all}\ r$$

(20)

$$\frac{\partial\theta}{\partial z} = \frac{\partial y_i}{\partial z} = 0\ \text{When}\ z = L,\ \text{for all}\ r$$

(21)

The procedure to calculate the heat transfer coefficient ("Uc") is detailed in the Supplementary Material. As previously mentioned, the models for this work were simulated for methane synthesis, which is expressed by Equation (22).

$$CO + 3H_2 \rightarrow CH_4 + H_2O$$

(22)

The model was studied for CO conversion and CH$_4$ formation, requiring only the calculation of concentration profiles of CO and CH$_4$. The rate of H$_2$ consumption will depend on the rates of CO consumption and CH$_4$ formation. Moreover, it will depend on the carbon number distribution of the ethane fraction (following the guidelines of Rodemerck

et al. [25]) according to the Schulz–Flory–Anderson distribution (as detailed in the Supplementary Material). The parameter will describe it for propane and the C_3/C_2 ratio known for ethane. These parameters were considered constant, irrespective of the rector's position and time. The selectivity of hydrocarbons was calculated based on the reaction rate of propane according to the Schulz–Flory–Anderson distribution, which depends on the reaction rate expressions of CH_4, and CO. Selectivity parameters are dependent on the temperature and the partial pressure of CO and H_2. In this regard, the reaction rate expressions are found in the Supplementary Material.

The relative simplicity of the equation proposed by Yates and Satterfield [26] was chosen as the basis of calculation for the rate of CO consumption (see Equation (23)) because it showed good correlations with the experimental data. The same relationship was recommended for calculating methane formation, as indicated in Equation (24).

$$-r_{CO} = \frac{(1-\beta_{co}t)A'_{co}e^{E_{co}/RT_o(\frac{1-\theta}{\theta})}y_{co}y_{H_2}}{(1+K_{co}y_{co})^2} \tag{23}$$

$$r_{CH_4} = \frac{(1-\beta_{CH4}t)A'_{CH_4}e^{E_{CH_4}/RT_o(\frac{1-\theta}{\theta})}y_{CO}^{1/2}y_{H_2}}{(1-K_{co}y_{co})^2} \tag{24}$$

Once the equations of state and the reaction stoichiometry had been determined, the different equations were entered into FlexPDE. The mesh was defined with 1200 nodes along two dimensions: radial (r) and axial (z).

2.4. 3-D dynamic Model

A 3-D representation of 1/8 of one cylindrical packed-bed reactor was drawn in AutoCAD and imported into COMSOL Multiphysics. Given that COMSOL renders results for the entire cylindrical geometry using axial symmetry, only 1/8 of the entire geometry was utilized to reduce the computational calculation cost of the simulation. The Brinkman equation for fluid transport in porous media (Brinkman Equations module, br) [27] was utilized to solve the flowing fluid in the reactor. To determine the concentration profiles, the advection–dispersion–reaction equation (Transport of Diluted Species in Porous Media module, tds; and Reacting Flow Diluted Species module, rfd) [27] was incorporated into the model to represent the mass transfer processes of reactants and products. The heat transfer equation (Heat Transfer in Porous Media module, het) [27] was also incorporated into the model to determine the temperature profile.

The physicochemical parameters for each module were the same as those utilized in the above-described models. Once the modules were set up, a mesh size analysis was performed to determine the element size that minimizes the Mean-Absolute-Error (MAE) relative to the experimental data, as indicated in the Supplementary Material. The mesh type that minimized the MAE was the "Extremely fine". The 3-dimensional geometry was discretized to 2400 elements and 765 nodes for this mesh.

In this section, the physicochemical parameters of the system to be studied and its components are presented. It included fluid, species, packed-bed and catalyst, heat and mass transfer coefficients, and reaction coefficients. All these values are required to define the models. Tables 1 and 2 show the experimental parameters used in the model extracted from Skaare [24].

Table 1. The reactor and catalyst dimensions and physicochemical properties.

Properties	Value
L (m)	1.5
R (m)	12.5×10^{-3}
R_o (m)	17.5×10^{-3}
ρ_b (kg/m^3)	0.89×10^3
ρ_p (kg/m^3)	1.59×10^3
ε_0	0.44
ε_p	0.485
d_p (m)	3.3×10^{-3}
C_{ps} (J/(kg K))	965
λ_p (W/(m K))	0.4
α_w (W/(m^{3}K))	430
λ_w (W/(m K))	18.0

Table 2. The fluid and gas conditions, dimensionless numbers, and kinetic parameters considered in simulations.

Fluid Properties		Dimensionless Numbers		Masic Peclets		Kinetic Parameters	
T_o(K)	498	Re_P	119	$1/Pe'_{mz}CO$	0.00111	K_{CO}	1.2
P_T(MPa)	1	Pr	0.57	$1/Pe'_{mz}H_2$	0.00112	E_{CO}	110
P_{N2}(MPa)	0.77	Sc_{CO}	0.8945	$1/Pe'_{mz}CH_4$	0.00111	E_{CH4}	140
u_o(m/s)	0.16	Sc_{H2}	0.2451	$1/Pe'_{mr}CO$	2.54486	A'_{CO}	0.0041
Co_{N2}(mol/m^3)	186	Sc_{CH4}	0.8155	$1/Pe'_{mr}H_2$	2.74323	A'_{CH4}	0.0006
Co_{CO}(mol/m^3)	17.4			$1/Pe'_{mr}CH_4$	2.55211	β_{CO}	0.0043
Co_{H2}(mol/m^3)	38.2					β_{CH4}	0.0097
Physical properties of gas mixture		Distribution parameters		Caloric Peclets		Thermal conductivity	
ϱ_g(kg/m^3)	5.77	α	0.69	$1/Pe'_{hz}$	0.00196	λ_{cr}(W/(mK))	0.6172
C_{pg}(J/(kg/K)	1333	γ	0.88	$1/Pe'_{hr}$	4.81445	U_c(W/(m^{2}K))	525.12
μ_g(Ns/m^2)	2.56×10^{-5}						
λ_g(W/(mK))	0.05972						

3. Results and Discussion

3.1. Analysis and Validation of the 2-D Stationary Model and the 3-D Dynamic Model

Figure 2a shows the CO concentration of the stationary 2-dimensional model (FlexPDE), dynamic 3-dimensional model (COMSOL), and the experimental data. Since there is no gradient of experimental concentrations through the radial axis, the profiles in the center of the bed were compared with the experimental one. For the stationary 2-dimensional model, we can observe good agreement between simulation and experimentation at distances close to the entrance of the bed in the axial direction. However, differences are observed as we move further away from the entrance in the axial direction. This is because the simulated data for the stationary model do not consider the variation in the catalyst activity, which decreases over time. This activity is proportionally related to the reaction rate [28], which will be lower.

Consequently, the simulated data for the stationary model present lower concentrations than the experimental ones; by not considering the decrease in catalyst activity, the conversion of CO increases, as shown in the previous figure. For example, the simulated CO concentration at the reactor outlet is 9 mol/m^3, while the experimental one is kept at 11.5 mol/m^3. For the dynamic 3-D model, the simulation agrees with the experimental data, following the same trend and showing a maximum discrepancy of ~15%, which is in line with Shin et al. [29].

On the other hand, Figure 2b shows the simulated and experimental CH_4 concentrations in the axial direction of the reactor. For the stationary 2-D model, CH_4 simulated concentration is in good agreement with the experimental data at a distance close to the entrance of the bed in the axial direction. Likewise, differences are observed as we move further away from the entrance in the axial direction. Again, this difference between the experimental and simulated concentration increases because the stationary model does not consider catalyst activity changes over time. For example, the CH_4 concentration at the reactor outlet is 0.9 mol/m^3, while the simulated one is 1.4 mol/m^3. This is because the reaction rate is higher when the catalyst activity factor is not considered since this factor is less than 1 [30]. Consequently, for a product such as CH_4, the simulated concentration will be greater than the experimental concentration since the former has a higher reaction rate, thus showing a more significant transformation of reactants to products [31]. For the dynamic 3-dimensional model, the simulation agrees with the experimental data, following the same trend and showing a maximum discrepancy of ~15%, also in concordance with Shin et al. [29].

The simulated and experimental temperature in the reactor center shows these results in Figure 2c. We can see that the simulated data differ from the experimental data by ~5 degrees. The difference between simulated and experimental values is due to two reasons: temperature measurements will depend on the heat capacity of the thermocouple that will affect the temperature data collection and the difficulty of taking the data for such a small radius of tube (1.25 cm). The experimental and simulated data have the same trend, as shown in Figure 2c, making the model valid. Furthermore, due to the tendency of the experimental data to present a maximum temperature point near the bed entrance, the theory proves that the reaction rate will be higher, which was also indicated by Irani et al. [32].
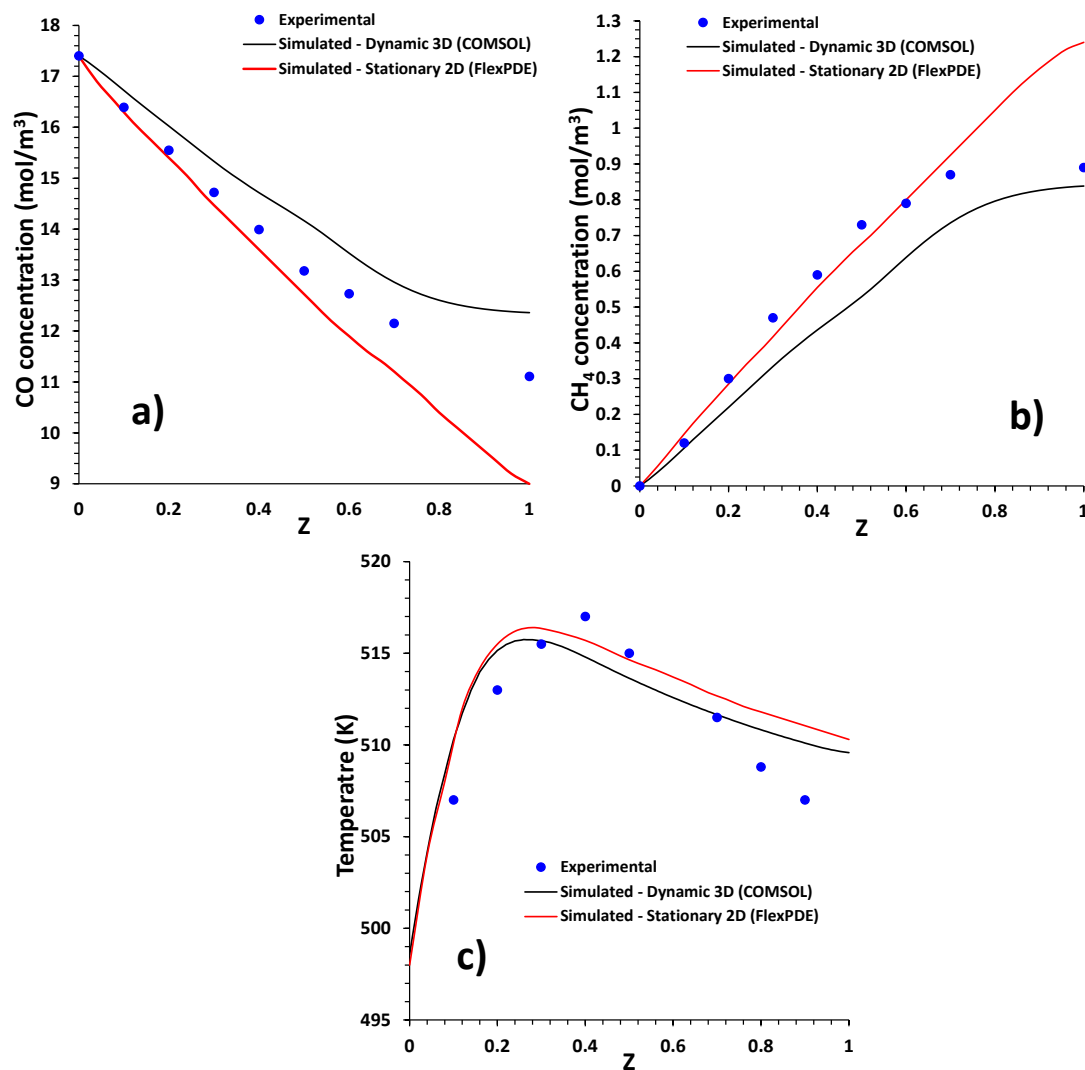
Figure 2. The simulated and experimental data for the 2-D stationary and the 3-D dynamic models: (**a**) CO concentration, (**b**) CH_4 concentration, and (**c**) Temperature.

3.2. *Analysis and Validation of the 1-D Dynamic Model and the 3-D Dynamic Model*

Figure 3 includes the simulation results of the dynamic 1-dimensional model. Figure 3a compares the experimental and simulated values considering the 1-dimensional model. It is observed that the simulated concentration values are higher than the experimental ones, which means that the CO did not react enough in the simulation. This is because the reaction rate is lower for the one-dimensional model than for the two-dimensional one, which is the one that is closest to reality. CO did not react enough in the simulation because the one-dimensional model takes the radial average temperature to calculate the reaction rate (in line with Kuncharam and Dixon [33]).

In contrast, the two-dimensional model takes the reaction rate in two dimensions. Therefore, the one-dimensional model will present less conversion than the two-dimensional model. Consequently, it can be concluded that the two-dimensional model presents better results and is the one that is closer to reality than the one-dimensional one.

Figure 3b shows the CH_4 concentration profile in the axial direction for the 1-dimensional model. The CH_4 concentration is lower for the simulation relative to the experiments. The experimental CH_4 concentration at the reactor outlet was 0.9 mol/m^3, while the simulated one was 0.7 mol/m^3. Both are different because not enough CO reacted to produce CH_4 to concentrations close to those observed experimentally.
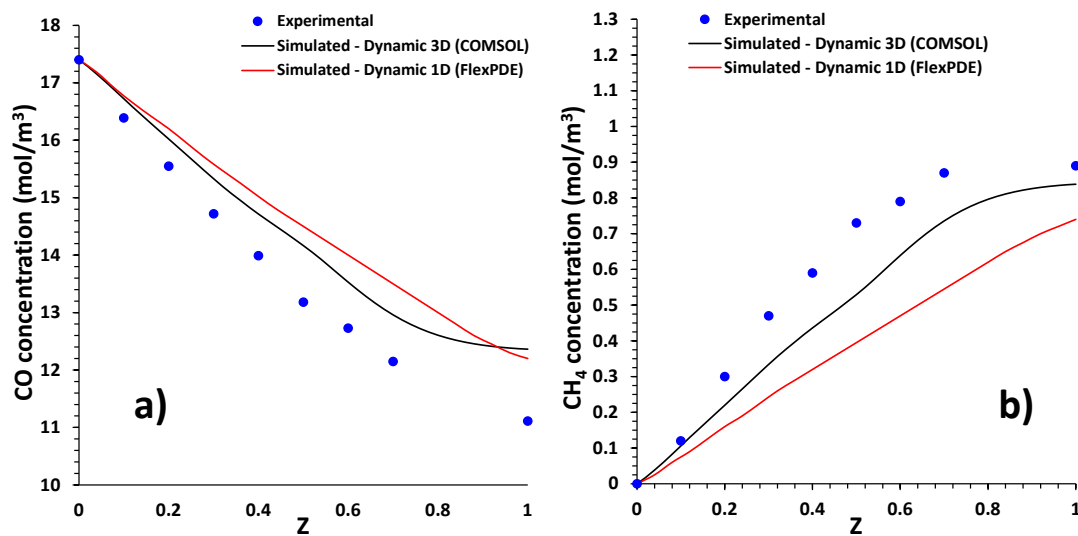
Figure 3. The simulated and experimental data for the 1-D dynamic and the 3-D dynamic models: (**a**) CO concentration, and (**b**) CH_4 concentration.

3.3. Analysis and Validation of the 2-D Dynamic Model and the 3-D Dynamic Model

Figure 4 includes the simulation results for the dynamic 2-dimensional model. Figure 4a compares the simulated and experimental CO mol/m^3 concentrations. Both the dynamic 2-dimensional and the 3-dimensional models agree with the experimental data. It is observed that when taking a dynamic model, the approximation of simulated and experimental data improves, as also explained by Mandić et al. [34]. This is mainly because the activity of the catalyst is considered over time. Thus, it loses its activity and causes the reaction rate to slow down, which is closer to reality. The experimental CO concentration at the reactor outlet was 11.5 mol/m^3, while the simulated one was 10.7 mol/m^3.

Figure 4b shows the comparison of simulated and experimental CH_4 concentrations. Both the dynamic 2-dimensional and the 3-dimensional models agree with the experimental data. The experimental CH_4 concentration at the reactor outlet was 0.9 mol/m^3, while the simulated one was 1.1 mol/m^3. Figure 4 shows that the dynamic 2-dimensional and the dynamic 3-dimensional models agree with the experimental data.
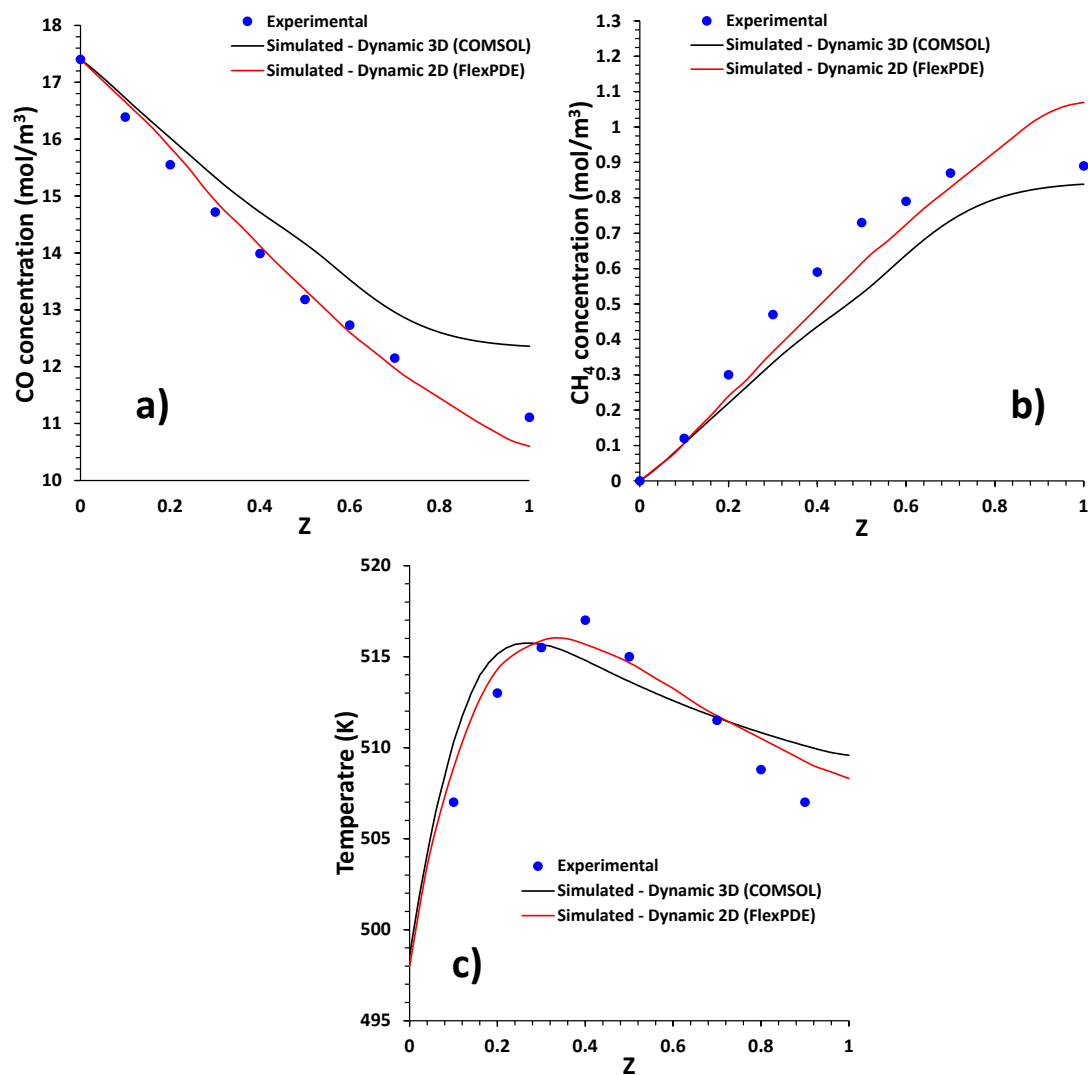
Figure 4. The simulated and experimental data for the 2-D dynamic and the 3-D dynamic models: (**a**) CO concentration, (**b**) CH_4 concentration, and (**c**) Temperature.

Figure 5 shows the temperature variation in the radial and axial directions for the dynamic 2-dimensional (Figure 5a) and the dynamic 3-dimensional model (Figure 5b). On the other hand, Figure 6 shows the reaction rate of CO in the radial and axial directions for both the dynamic 2-dimensional (Figure 6a) and the dynamic 3-dimensional model (Figure 6b). Figure 5a,b follow the same trend as Figure 6a,b. This reflects that increased/decreased temperatures imply increased/decreased reaction rates. The geometry built and utilized to construct the dynamic 3-dimensional model in COMSOL is available in the Supplementary Material.
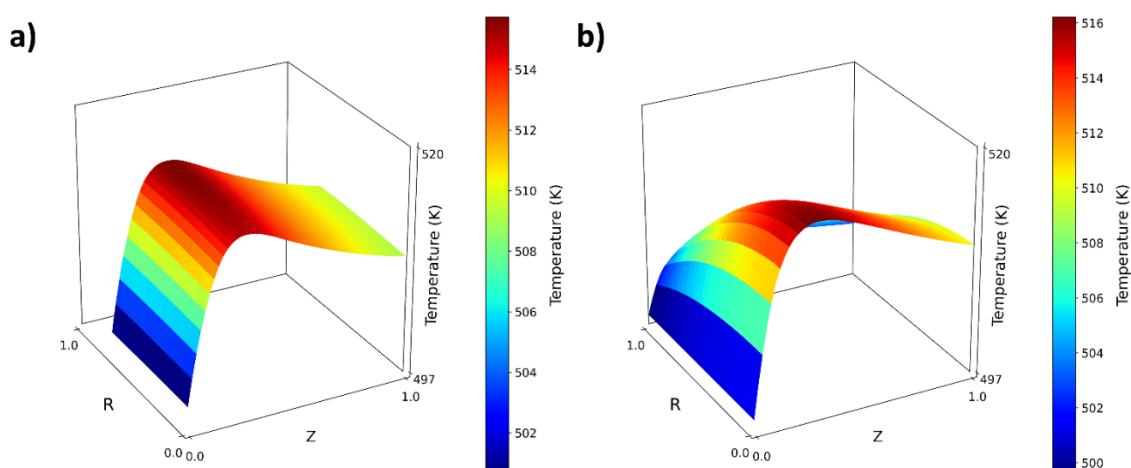
Figure 5. Bed temperature for (**a**) 3-dimensional dynamic model (COMSOL), and (**b**) 2-dimensional dynamic model (FlexPDE).
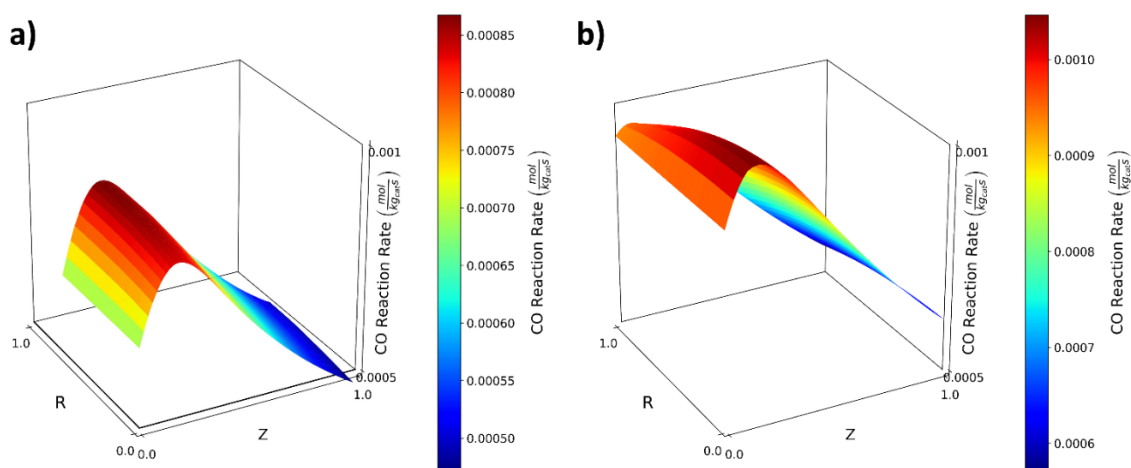

Figure 6. The CO Reaction Rate (mol/kg$_{cat}$ s) for (**a**) 3-dimensional dynamic model (COMSOL), and (**b**) 2-dimensional dynamic model (FlexPDE).

4. Conclusions

In this work, the thermochemical analysis of a cylindrical packed-bed reactor was carried out using the finite element methodology. Different CFD software such as FlexPDE and COMSOL Multiphysics was employed. Several approaches considering stationary and dynamic simulations and a multi-dimensional study were proposed for methane production using the F-T synthesis. The 1-D and 2-D simulations performed with FlexPDE and the 3-D simulation from COMSOL were compared to experimental data resulting in an excellent agreement, validating the concentrations of CO and CH$_4$ and the temperature profiles. In the axial direction, both stationary and dynamic schemes described the experimental phenomena accurately.

On the other hand, surface responses for temperature and CO reaction rate were developed to observe the dependence of axial and radial directions. In this regard, although similar trends were observed when comparing FlexPDE and COMSOL models, there were few differences, which can be attributed to the different types of transport equations employed. For instance, FlexPDE models were built based on dispersion models using the Peclet number, which seems to be more sensitive to heat transfer as the temperature was not as stable as the COMSOL model.

Since a comparison between different CFD modeling software is proposed in this work, it can be suggested that it would be interesting to consider Ansys Fluent for further studies. This software also provides some heat transfer models for porous media, like the

non-equilibrium thermal model, which focuses on the fluid and the catalyst treated separately. As aforementioned, in real applications, both phases are not supposed to be at thermal equilibrium, so more equations must be solved in these cases.

Modeling reactors using heterogenous catalysts can be divided into a) transport phenomena and b) kinetic modeling. These two areas interact to predict temperature profiles and concentrations in space and time. This study uses COMSOL and FlexPDE to model the heat and mass transfer and the kinetics of the reactor. This manuscript uses F-T as a reaction example which has simple reaction kinetics; however, this study can serve as starting point to model more complex reactions and will allow readers to use it as a basis for more detailed models.

Nomenclature

A'_i	Modified exponential factor for species i in the Arrhenius expression	
a_v	External surface area per unit volume of the bed	
C_i	Concentration of species i in the fluid phase	mol/m³
C_{0i}	Initial concentration of the species i	mol/m³
C_{si}	Concentration of species i in the solid phase	mol/m³
Co_{si}	Initial concentration on the surface	mol/m³
c_{pg}	Heat capacity of the fluid phase	J/(kgK)
c_{ps}	Heat capacity of the fluid phase	J/(kgK)
d_p	Equivalent particle diameter,	m
d_t	Tube diameter	m
E_i	Activation energy for species i	J/mol
ΔH_i	Enthalpy of reaction	J
h_c	Coefficient of heat transfer between solid and fluid phase	W/m³K
k_c	Mass transfer coefficient between solid and fluid phase	m/s
k_p	Reaction constant for the Ficher-Tropsch polymerization	
k_t	Reaction constant for the determination of Ficher-Tropsch	
L	Bed length	m
Nu	Nusselt number	
Nu_w	Nusselt number	
P	Pressure	MPa
Po	Initial Pressure	MPa
P_i	Partial pressure for species i	MPa
Pe_h	Peclet number of heat	
Pe^o_h	Molecular Peclet number of heat based on particle diameter	
Pe_{hv}	Radial effective heat peclet number based on particle diameter	
Pe_{hz}	Axial effective heat peclet number based on particle diameter	
Pe'_{hv}	Radial effective Peclet number of heat based on bed dimensions	
Pe'_{hz}	Axial effective Peclet number of heat based on bed dimensions	

Pe_{mv}	Radial effective Peclet number of mass based on particle diameter	
Pe_{mz}	Effective axial Peclet number of mass based on particle diameter	
Pe'_{mr}	Radial effective Peclet number of mass based on bed dimensions	
Pe'_{mz}	Radial effective Peclet number of mass based on bed dimensions	
Pr	Prandlt number	
R	Internal radius of tube	m
R_0	External radius of tube	m
R'	Ratio of the internal radius of the tube to the particle diameter	
Re_P	Reynolds number based on particle diameter	
R_t	Radius of tube	m
r	Radial coordinate	m
r'	Dimensionless Radial coordinate	
r_n	Reaction rate of formation of n alkanes	
r_{vi}	Reaction rate of species i	mol/(kgcat s)
$(-\Delta H)_{rv}$	Total heat generation by reaction	W/kg cat
S_n	Selectivity of n-alkanes	
Sc	Schmidt number	
Sh	Sherwood number	
T	Fluid temperature	K
T_0	Initial fluid temperature	K
T_s	Solid Temperature	K
T_{os}	Solid initial temperature	K
T_c	Cooling liquid temperature	K
T_w	Wall temperature	K
t	Time	h
U	Total Heat Transfer Coefficient for one dimension,	W/(m²K)
U_c	Total Heat Transfer Coefficient	W/(m²K)
u	Velocity, m/s	
u_0	Average speed	m/s
V_P	Volume of the particle	m
X	Axial dimensionless coordinate z/L in the graphs	
Y	Radial dimensionless r/R coordinate in graphs	
y_i	Dimensionless concentration of species i, C_i/C_{io}	
z	Axial coordinate	m
z'	Dimensionless Axial coordinate z/L	

Greek Letters

α	Probability constant for the alkane chain to grow	
α_w	Heat Transfer coefficient through the wall	
βi	Deactivation coefficient for species i	1/h
γ	C2/C3 ratio	
ε	Local porosity	
ε_0	Average porosity	
ε_P	Porosity of the catalyst particle	
η	Effectiveness Factor	
λ^0_c	Thermal conductivity due to conduction	W/(mK)
λ^f_c	Thermal conductivity due to convection	W/(mK)
λ_{cr}	Mean radial thermal conductivity of the bed	W/(mK)
λ_{cz}	Mean axial thermal conductivity of the bed	W/(mK)
λ_f	Thermal conductivity of the fluid phase	W/(mK)
λ_P	Thermal conductivity through the particle	W/(mK)
λ_w	Thermal conductivity of the bed wall	W/(mK)
μ_g	Fluid Viscosity	Ns/m²
θ	Adimensional Temperature T/To	
θ_c	Dimensionless temperature of the cooling fluid Tc/To	
ϱ_b	Density of the catalyst based on the volume of the bed	kg/m³
ϱ_g	Density of the fluid phase	kg/m³
ϱ_ϱ	Density of the catalyst particle	kg/m³

References

1. Perry, R.; Green, D.; Maloney, J. *Perry's Chemical Engineers' Handbook*; 7th ed.; McGraw-Hill: Madrid, Spain, 2001; ISBN 84-481-3008-1.
2. Cocco, R.; Karri, S.; Prog, T.K.-C.E.; 2014, U. Introduction to Fluidization. *Chem. Eng. Prog.* **2014**, *110*, 21–29.
3. Fratalocchi, L.; Groppi, G.; Visconti, C.G.; Lietti, L.; Tronconi, E. Packed-POCS with Skin: A Novel Concept for the Intensification of Non-Adiabatic Catalytic Processes Demonstrated in the Case of the Fischer-Tropsch Synthesis. *Catal. Today* **2022**, *383*, 15–20. https://doi.org/10.1016/J.CATTOD.2020.12.031.
4. Merino, D.; Sanz, O.; Montes, M. Effect of the Thermal Conductivity and Catalyst Layer Thickness on the Fischer-Tropsch Synthesis Selectivity Using Structured Catalysts. *Chem. Eng. J.* **2017**, *327*, 1033–1042. https://doi.org/10.1016/J.CEJ.2017.07.003.
5. Calverley, E.M.; Witt, P.M.; Sweeney, J.D. Reactor Runaway Due to Statistically Driven Axial Activity Variations in Graded Catalyst Beds: Loading from Pre-Measured Single Tube Aliquots. *Chem. Eng. Sci.* **2013**, *90*, 170–178. https://doi.org/10.1016/J.CES.2012.12.017.
6. Philippe, R.; Lacroix, M.; Dreibine, L.; Pham-Huu, C.; Edouard, D.; Savin, S.; Luck, F.; Schweich, D. Effect of Structure and Thermal Properties of a Fischer–Tropsch Catalyst in a Fixed Bed. *Catal. Today* **2009**, *147*, S305–S312. https://doi.org/10.1016/J.CATTOD.2009.07.058.
7. Shah, Z.; Kumam, P.; Ullah, A.; Khan, S.N.; Selim, M.M. Mesoscopic Simulation for Magnetized Nanofluid Flow within a Permeable 3D Tank. *IEEE Access* **2021**, *9*, 135234–135244. https://doi.org/10.1109/ACCESS.2021.3115599.
8. Visconti, C.G.; Tronconi, E.; Lietti, L.; Groppi, G.; Forzatti, P.; Cristiani, C.; Zennaro, R.; Rossini, S. An Experimental Investigation of Fischer–Tropsch Synthesis over Washcoated Metallic Structured Supports. *Appl. Catal. A Gen.* **2009**, *370*, 93–101. https://doi.org/10.1016/J.APCATA.2009.09.023.
9. Asalieva, E.; Gryaznov, K.; Kulchakovskaya, E.; Ermolaev, I.; Sineva, L.; Mordkovich, V. Fischer–Tropsch Synthesis on Cobalt-Based Catalysts with Different Thermally Conductive Additives. *Appl. Catal. A Gen.* **2015**, *505*, 260–266. https://doi.org/10.1016/J.APCATA.2015.08.006.
10. Fratalocchi, L.; Visconti, C.G.; Groppi, G.; Lietti, L.; Tronconi, E. Intensifying Heat Transfer in Fischer-Tropsch Tubular Reactors through the Adoption of Conductive Packed Foams. *Chem. Eng. J.* **2018**, *349*, 829–837. https://doi.org/10.1016/J.CEJ.2018.05.108.
11. Chandra, V.; Vogels, D.; Peters, E.A.J.F.; Kuipers, J.A.M. A Multi-Scale Model for the Fischer-Tropsch Synthesis in a Wall-Cooled Packed Bed Reactor. *Chem. Eng. J.* **2021**, *410*, 128245. https://doi.org/10.1016/J.CEJ.2020.128245.
12. Dixon, A.G.; Van Dongeren, J.H. The Influence of the Tube and Particle Diameters at Constant Ratio on Heat Transfer in Packed Beds. *Chem. Eng. Process. Process Intensif.* **1998**, *37*, 23–32. https://doi.org/10.1016/S0255-2701(97)00033-0.
13. Mohammad, N.; Chukwudoro, C.; Bepari, S.; Basha, O.; Aravamudhan, S.; Kuila, D. Scale-up of High-Pressure F-T Synthesis in 3D Printed Stainless Steel Microchannel Microreactors: Experiments and Modeling. *Catal. Today* **2021**, *397–399*, 182–196. https://doi.org/10.1016/J.CATTOD.2021.09.038.
14. Abusrafa, A.E.; Challiwala, M.S.; Wilhite, B.A.; Elbashir, N.O. Thermal Assessment of a Micro Fibrous Fischer Tropsch Fixed Bed Reactor Using Computational Fluid Dynamics. *Processes* **2020**, *8*, 1213. https://doi.org/10.3390/PR8101213.
15. Chabot, G.; Guilet, R.; Cognet, P.; Gourdon, C. A Mathematical Modeling of Catalytic Milli-Fixed Bed Reactor for Fischer–Tropsch Synthesis: Influence of Tube Diameter on Fischer Tropsch Selectivity and Thermal Behavior. *Chem. Eng. Sci.* **2015**, *127*, 72–83. https://doi.org/10.1016/J.CES.2015.01.015.
16. Na, J.; Kshetrimayum, K.S.; Lee, U.; Han, C. Multi-Objective Optimization of Microchannel Reactor for Fischer-Tropsch Synthesis Using Computational Fluid Dynamics and Genetic Algorithm. *Chem. Eng. J.* **2017**, *313*, 1521–1534. https://doi.org/10.1016/J.CEJ.2016.11.040.
17. Pavlišič, A.; Ceglar, R.; Pohar, A.; Likozar, B. Comparison of Computational Fluid Dynamics (CFD) and Pressure Drop Correlations in Laminar Flow Regime for Packed Bed Reactors and Columns. *Powder Technol.* **2018**, *328*, 130–139. https://doi.org/10.1016/J.POWTEC.2018.01.029.
18. Amiri, L.; Ghoreishi-Madiseh, S.A.; Hassani, F.P.; Sasmito, A.P. Estimating Pressure Drop and Ergun/Forchheimer Parameters of Flow through Packed Bed of Spheres with Large Particle Diameters. *Powder Technol.* **2019**, *356*, 310–324. https://doi.org/10.1016/J.POWTEC.2019.08.029.
19. Khan, S.; Selim, M.M.; Gepreel, K.A.; Ullah, A.; Ikramullah; Ayaz, M.; Mashwani, W.K.; Khan, E. An Analytical Investigation of the Mixed Convective Casson Fluid Flow Past a Yawed Cylinder with Heat Transfer Analysis. *Open Phys.* **2021**, *19*, 341–351. https://doi.org/10.1515/PHYS-2021-0040/MACHINEREADABLECITATION/RIS.
20. Rai, A.; Anand, M.; Farooqui, S.A.; Sibi, M.G.; Sinha, A.K. Kinetics and Computational Fluid Dynamics Study for Fischer–Tropsch Synthesis in Microchannel and Fixed-Bed Reactors. *React. Chem. Eng.* **2018**, *3*, 319–332. https://doi.org/10.1039/C8RE00018B.
21. Oñate, W.; Maldonado, S.; Taco, S.; Caiza, G. Computational Fluid Dynamic Simulation with Experimental Validation in Turbine Pipeline. *Int. J. Recent Technol. Eng.* **2019**, *8*, 927–931.
22. Deutschmann, O. Modeling of the Interactions Between Catalytic Surfaces and Gas-Phase. *Catal. Lett.* **2014**, *145*, 272–289. https://doi.org/10.1007/S10562-014-1431-1.
23. Pessoa, D.R.; Finkler, A.T.J.; Machado, A.V.L.; Mitchell, D.A.; de Lima Luz, L.F. CFD Simulation of a Packed-Bed Solid-State Fermentation Bioreactor. *Appl. Math. Model.* **2019**, *70*, 439–458. https://doi.org/10.1016/J.APM.2019.01.032.

24. Skaare, S. Reaction and Heat Transfer in a Wall-Cooled Fixed Bed Reactor, University of Trondheim, The Norwegian Institute of Technology, Laboratory of Industrial Chemistry, [Thesis submitted for the Doctor of Engineering degree]. **1993**. http://www.fischer-tropsch.org/DOE/DOE_reports/95717546/de95717546_toc.htm

25. Rodemerck, U.; Holeňa, M.; Wagner, E.; Smejkal, Q.; Barkschat, A.; Baerns, M. Catalyst Development for CO2 Hydrogenation to Fuels. *ChemCatChem* **2013**, *5*, 1948–1955. https://doi.org/10.1002/CCTC.201200879.

26. Yates, I.C.; Satterfield, C.N. Intrinsic Kinetics of the Fischer-Tropsch Synthesis on a Cobalt Catalyst. *Energy Fuels* **2002**, *5*, 168–173. https://doi.org/10.1021/EF00025A029.

27. Introduction to the Porous Media Flow Module User's Guide, pp. 6-38. COMSOL Multiphysics® v. 5.5. COMSOL AB, Stockholm, Sweden. 2019.

28. Vervloet, D.; Kapteijn, F.; Nijenhuis, J.; Van Ommen, J.R. Fischer–Tropsch Reaction–Diffusion in a Cobalt Catalyst Particle: Aspects of Activity and Selectivity for a Variable Chain Growth Probability. *Catal. Sci. Technol.* **2012**, *2*, 1221–1233. https://doi.org/10.1039/C2CY20060K.

29. Shin, M.S.; Park, N.; Park, M.J.; Jun, K.W.; Ha, K.S. Computational Fluid Dynamics Model of a Modular Multichannel Reactor for Fischer–Tropsch Synthesis: Maximum Utilization of Catalytic Bed by Microchannel Heat Exchangers. *Chem. Eng. J.* **2013**, *234*, 23–32. https://doi.org/10.1016/J.CEJ.2013.08.064.

30. Guettel, R.; Turek, T. Comparison of Different Reactor Types for Low Temperature Fischer–Tropsch Synthesis: A Simulation Study. *Chem. Eng. Sci.* **2009**, *64*, 955–964. https://doi.org/10.1016/J.CES.2008.10.059.

31. Moazami, N.; Wyszynski, M.L.; Mahmoudi, H.; Tsolakis, A.; Zou, Z.; Panahifar, P.; Rahbar, K. Modelling of a Fixed Bed Reactor for Fischer–Tropsch Synthesis of Simulated N2-Rich Syngas over Co/SiO2: Hydrocarbon Production. *Fuel* **2015**, *154*, 140–151. https://doi.org/10.1016/J.FUEL.2015.03.049.

32. Irani, M.; Alizadehdakhel, A.; Pour, A.N.; Proulx, P.; Tavassoli, A. An Investigation on the Performance of a FTS Fixed-Bed Reactor Using CFD Methods. *Int. Commun. Heat Mass Transf.* **2011**, *38*, 1119–1124. https://doi.org/10.1016/J.ICHEATMASSTRANSFER.2011.05.005.

33. Kuncharam, B.V.R.; Dixon, A.G. Multi-Scale Two-Dimensional Packed Bed Reactor Model for Industrial Steam Methane Reforming. *Fuel Process. Technol.* **2020**, *200*, 106314. https://doi.org/10.1016/J.FUPROC.2019.106314.

34. Mandić, M.; Dikić, V.; Petkovska, M.; Todić, B.; Bukur, D.B.; Nikačević, N.M. Dynamic Analysis of Millimetre-Scale Fixed Bed Reactors for Fischer-Tropsch Synthesis. *Chem. Eng. Sci.* **2018**, *192*, 434–447. https://doi.org/10.1016/J.CES.2018.07.052.